

Constraint-induced breaking and restoration of ergodicity in spin-1 PXP models

Bhaskar Mukherjee,^{1,2,*} Zi Cai,^{1,3,4,†} and W. Vincent Liu^{2,1,5,4,6,‡}

¹*Wilczek Quantum Center, School of Physics and Astronomy, Shanghai Jiao Tong University, Shanghai 200240, China*

²*Department of Physics and Astronomy, University of Pittsburgh, Pittsburgh, PA 15260, USA*

³*Key Laboratory of Artificial Structures and Quantum Control, School of Physics and Astronomy, Shanghai Jiao Tong University, Shanghai 200240, China*

⁴*Shanghai Research Center for Quantum Sciences, Shanghai 201315, China*

⁵*T. D. Lee Institute, Shanghai Jiao Tong University, Shanghai 200240, China*

⁶*Shenzhen Institute for Quantum Science and Engineering, Southern University of Science and Technology, Shenzhen 518055, China*

(Dated: April 5, 2021)

Eigenstate Thermalization Hypothesis (ETH) has played a pivotal role in understanding ergodicity and its breaking in isolated quantum many-body systems. Recent experiment on 51-atom Rydberg quantum simulator and subsequent theoretical analysis have shown that hardcore kinetic constraint can lead to weak ergodicity breaking. In this work, we demonstrate, using 1d spin-1 PXP chains, that miscellaneous type of ergodicity can be realized by adjusting the hardcore constraints between different components of nearest neighbor spins. This includes ETH violation due to emergent shattering of Hilbert space into exponentially many subsectors of various sizes, a novel form of non-integrability with an extensive number of local conserved quantities and strong ergodicity. We analyze these different forms of ergodicity and study their impact on the non-equilibrium dynamics of a \mathbb{Z}_2 initial state. We use forward scattering approximation (FSA) to understand the amount of \mathbb{Z}_2 -oscillation present in these models. Our work shows that not only ergodicity breaking but an appropriate choice of constraints can lead to restoration of ergodicity as well.

PACS numbers:

INTRODUCTION

Eigenstate thermalization hypothesis (ETH) offers the most widely accepted mechanism of thermalization of local observables in out of equilibrium closed quantum many body systems [1–4]. An ETH satisfying system, prepared in an unentangled product state, gets strongly entangled quickly under its own dynamics, losing all the information of the initial state except the conserved quantities (e.g total energy). These systems are usually strongly interacting in nature which makes the full quantum system, though well isolated from external environment, suffer from the presence of an indigenous heat bath. This makes the study of ETH-violating systems not only of fundamental importance but also of technological importance from the perspective of quantum information protection, quantum state preparation and preservation of quantum coherence (which is the measure of quantumness of a system) up to very long time.

Integrable systems [5], possessing an extensive number of conserved quantities, have long been known to disobey ETH. A prototypical example is transverse field Ising model (TFIM) which though appears an interacting system in original spin language, becomes a free system via Jordan-Wigner transformation [6]. Many body localized (MBL) systems [7] which are mostly one-dimensional interacting quantum system with onsite disorder potential, forms another class of ETH violating system and has been studied in detail over the last decade. These systems are examples where we see strong violation of ETH

in the sense all eigenstates violates ETH.

Recently, anomalous oscillation from a density wave (\mathbb{Z}_2) state observed in a quench dynamics experiment using a 51-atom Rydberg quantum simulator [8] has revitalized the interest into the field of thermalization and its violation. This phenomenon is understood by using spin-1/2 PXP model which hosts extensive number of ETH violating states with high \mathbb{Z}_2 -overlap, dubbed as quantum many body scars, in its spectrum[9]. So far, a plethora of study [11–14] has not only revealed the full phenomenology of the scar states but they have been found in a variety of models ranging from different spin models [15, 16], Hubbard models [17], higher spin PXP models[19, 20], Floquet systems [21], disordered systems [22], quantum Hall system [23], in higher dimension [24], via confinement [25] etc. In many of these studies scar states are exactly constructed either in matrix product state (MPS) form or by repeatedly acting suitably designed creation operator on some mother state. These kind of construction quite straightforwardly explains the ETH violating nature of the scar states. But in spite of being the first experimentally realized model to host quantum many body scar, a fully satisfactory explanation of scarring in PXP model is still a open problem. Except a few scar states for which exact MPS representation was obtained [11], numerics and semi-analytical techniques like forward scattering approximation [9, 10, 14], single-mode approximation [26] etc are the only option to study the majority number of scar states in PXP model.

The spin-1 PXP model [19, 20] is defined by the Hamiltonian : $H = -\sum_i \mathcal{P}S_i^x\mathcal{P}$ in a chain of L sites where the local (per site) Hilbert space is spanned by the eigenstates of S^z ($|m\rangle \equiv |-\rangle, |0\rangle, |+\rangle$ for $m = -1, 0, +1$) and the operator $\mathcal{P} = \prod_i \mathcal{P}_{i,i+1}$ characterizes the constrained Hilbert space. In traditional spin-1 PXP [19] model at least one of two consecutive spin must be in the $|-\rangle$ state which fixes the form of the projector : $\mathcal{P}_{i,i+1} = P_i + P_{i+1} - P_i P_{i+1}$ with $P_i = |-\rangle_i \langle -|_i$. This means, $|00\rangle, |+0\rangle, |0+\rangle$ and $|++\rangle$ type of configurations are not allowed in the constrained Hilbert space (\mathbb{H}^{PXP}). This opens up the question that what happen when different set of constraints are used. In this work we show that the many body spectrum of spin-1 PXP model can get dramatically changed when certain constraints are abolished. To this end we consider three different set of constraints and construct three corresponding model Hamiltonians.

Three Models: Model-I, II & III are defined by the following Hamiltonians

$$H^\alpha = \sum_{i=1}^L \mathcal{P}^\alpha S_i^x \mathcal{P}^\alpha \quad (1)$$

where $\mathcal{P}^\alpha = \prod_i \mathcal{P}_{i,i+1}^\alpha$ for $\alpha = I, II, III$ and $\mathcal{P}_{i,i+1}^I = \mathcal{P}_{i,i+1} + [(|+\rangle\langle +|)_i \otimes (|+\rangle\langle +|)_{i+1}]$, $\mathcal{P}_{i,i+1}^{II} = \mathbb{I}_i \otimes \mathbb{I}_{i+1} - [(|0\rangle\langle 0|)_i \otimes (|0\rangle\langle 0|)_{i+1}]$, $\mathcal{P}_{i,i+1}^{III} = \mathcal{P}_{i,i+1}^{II} - [(|+\rangle\langle +|)_i \otimes (|+\rangle\langle +|)_{i+1}]$. Note that, these three models are also in PXP form, but to distinguish them from traditional spin-1 PXP model we use the model index (α) in the superscript.

In Fig.1 we show how these models can be obtained by imposing specific constraints over a spin-1 free paramagnet ($H = \sum_i S_i^x$) or abolishing specific constraints from traditional spin-1 PXP model. We find that if we allow $|++\rangle$ configurations on top of \mathbb{H}^{PXP} , which we call Model-I, the spectrum gets shattered into exponentially many emergent subsectors of different size including \mathbb{H}^{PXP} as one of the largest block. If we further allow $|+0\rangle/|0+\rangle$ type configurations (Model-II), an extensive number of local conserved quantities arises. This does not make Model-II exactly solvable due to some degeneracies in the spectrum of the conserved quantities. In fact, we find that these conserved quantities can be used atmost to label different sectors of Model-II which are nothing but disconnected patches of spin-1/2 PXP model of different sizes. If we add $|++\rangle$ type configurations on top of Model-II, all the scar states disappear and the spectrum become strongly ergodic (Model-III). We demonstrate the consequence of these different type of ergodicity in the non-equilibrium dynamics of the \mathbb{Z}_2 state. Finally we use FSA to understand the degree of \mathbb{Z}_2 -oscillation as well as ergodic nature of these three models.

The symmetries of these Hamiltonians include translation, inversion about center bond/site and particle-hole symmetry characterized by the vanishing anticommuta-

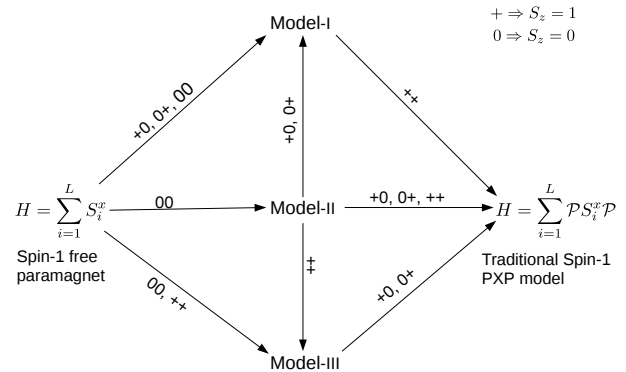


FIG. 1: Schematic picture of construction of Model-I, II & III by imposing (along the arrow direction) constraints on the Hilbert space of a spin-1 free paramagnet and abolishing (opposite to the arrow direction) constraints from traditional spin-1 PXP model. The constraints (forbidden configurations on a pair of adjacent sites) are shown on top of the arrows.

tor of the operator $\mathcal{C} = \prod_i (2(S_i^z)^2 - I_i)$ with the Hamiltonians : $\{H^\alpha, \mathcal{C}\} = 0$ for $\alpha = I, II, III$. The last symmetry guarantees that if there is an eigenstate ψ at energy E then there will also be an eigenstate ($\mathcal{C}|\psi\rangle$) at $-E$. The Hilbert space dimension grows much slowly than naive 3^L depending on the nature of constraints and choice of boundary conditions (see Table.I). We utilize the first two symmetry and work in zero momentum and inversion symmetric ($K = 0, I = +1$) sector to access largest possible system. The intertwining of the particle-hole and inversion symmetry generates an exponentially large number of zero modes [27].

The spectrum of Model-I posses a lot of degeneracies at nonzero (including integers). We explore the connectivity of states in the Hilbert space of Model-I and find that it (even each momentum and inversion symmetry sector) is shattered into exponentially many emergent subsectors [28, 29](see Fig.2(a)). The lowest possible size (in S^z basis) of such emergent blocks is one, hence these are unentangled, zero energy eigenstates of H^I . These inert states remain frozen under the dynamics generated by the Hamiltonian. The number of such inert eigenstates (I_L) scales as $I_L \sim \phi^L$ in large L limit where $\phi = \frac{\sqrt{5}-1}{2}$ is the Fibonacci number and the proportionality constant depends on the choice of boundary condition (see [30]). The eigenstates in low (> 1) dimensional subsectors have very small but nonzero entanglement, some of them also have interesting properties like integer energy and magnetization. The minimally entangled states (in the central region of the spectrum) are eigenstates of a subsector of size 3×3 . These eigenstates (with energy $E = \pm 1, 0$) are given by $|\psi_E\rangle = \frac{1}{2}|\psi_-\rangle - \frac{e^{i\pi E}}{2}|\psi_+\rangle + \frac{E}{\sqrt{2}}|\psi_0\rangle$ where

	Model-I	Model-II	Model-III
Forbidden configurations	$ 00\rangle, +0\rangle, 0+\rangle$	$ 00\rangle$	$ 00\rangle, ++\rangle$
d_L^{OBC}	$\approx 2.247^L$	$\frac{(1-\sqrt{3})^L(\sqrt{3}-2)+(1+\sqrt{3})^L(\sqrt{3}+2)}{2\sqrt{3}} \approx 2.732^L$	$\frac{(1-\sqrt{2})^{L+1}+(1+\sqrt{2})^{L+1}}{2} \approx 2.414^L$
Feature	Emergent Hilbert space shattering	Exponentially many local conserved quantities ; non-integrable	Strongly Ergodic.

TABLE I: Hardcore constraints, scaling of Hilbert space dimension in open boundary condition (OBC)(see [30] for derivations) and main features of the spectrum of Model-I, II & III.

$|\psi_m\rangle = \frac{1}{\sqrt{L}} \sum_{n=1}^L T^n [\otimes_{i=1}^{L-3} |+\rangle_i \otimes |-m-\rangle]$; $m = \pm, 0$ and T is the translation operator. Red (blue) color is used to denote inert (active) sites. The half chain entanglement entropy ($S_{L/2}$) of these states are found to be $S_{L/2} = \ln(\frac{2L}{L-4}) + \frac{4}{L} \ln(\frac{L-4}{2})$ (see [30]) which assumes area law behavior in thermodynamic limit (see inset of Fig.2(b)). We also find that some special states with $E = \pm 2$ (belonging to subsectors of size 6×6) has logarithmic entanglement entropy ($S_{L/2} = \ln L - \ln 2$; see [30]). The magnetization ($S_z = \sum_{i=1}^L S_i^z$) of such eigenstates with energy $E = \pm n$ turns out to be $L - 5n$ which are non-negative at any system size as these type of states don't appear for $L < 5n$ (see [30]). This expectation value is much higher than the corresponding thermal average ($\langle S_z \rangle_\beta = Tr[\rho_\beta S_z]$ with $\rho_\beta = \exp(-\beta H^I)/Tr[\exp(-\beta H^I)]$) which is always negative due to the excessiveness of $|-\rangle$ compared to $|+\rangle$ states in the constrained Hilbert space of Model-I. Thus such states clearly violates ETH.

The number of $|++\rangle$ configurations ($N_{++} = \sum_i (|++\rangle\langle ++|)_{i,i+1}$) turns out to be a conserved quantity for Model-I which can be used to label (not uniquely) different subsectors. The block with $N_{++} = 0$ is nothing but the traditional spin-1 PXP model. Note that, this kinetic constraint (no two spin in $|+\rangle$ state can sit next to each other) is emergent in nature as the underlying Hamiltonian does not have it [32]. The block with $N_{++} = 1$ is the largest block in the largest possible system size ($L = 16$) we have explored numerically. Blocks with same N_{++} (> 1) can be further labeled by N_{+++} and so on. We note that there are many subsectors with $N_{++} > 1$ and $N_{+++} = 0$ whose states contains isolated $|++\rangle$ configurations, separated by active sites. Such subsectors can be further labeled by number of $|+-+ - ++\rangle$, $|+ + - - ++\rangle$ etc type of inert configurations. For example, at $L = 10$, there are 3 subsectors with ($N_{++} = 2, N_{+++} = 0$) which can be uniquely labeled by the quantum numbers (N_{++-++}, N_{++-++}) with values (0, 0), (0, 1) and (1, 0). For $L > 10$, number of such subsectors is > 3 , consequently unique labeling of them can not be achieved. In fact, projectors on inert configurations of all system sizes $\leq L$ are conserved quantities of a system of size L . Though the inert states are

unentangled, the projectors on them are nonlocal in nature. Moreover, their number scales exponentially with system size and thus an unique set of conserved quantities to distinguish different subsectors is lacking. That's why this is an emergent shattering of Hilbert space induced by the choice of constraints. We note that ETH violation due to emergent fragmentation of Hilbert space was first observed in fractonic circuit with local conservation of charge and dipole moment [28] and in the corresponding Hamiltonian system [29]. Subsequent works showed that Hilbert space fragmentation can also happen from strict confinement[31].

In Model-II only $|00\rangle$ type configurations are not allowed. The spectrum of Model-II also holds nonzero-energy-degeneracies inside the $K = 0, I = +1$ sector. This time we find an extensive ($= L$) number of local quantities (O_i) which commutes with the Hamiltonian, i.e $[O_i, H^{II}] = 0, \forall i$. We find that $O_i = (|+\rangle\langle -| + |0\rangle\langle 0| + |-\rangle\langle +|)_i = 2(S_i^x)^2 - \mathbb{I}_i$ (see [30]). Interestingly, this does not make Model-II completely integrable as each O_i have degenerate eigenstates. The eigenvalues of O_i are $(+1, +1, -1)$ with corresponding eigenstates $|O_1^+\rangle = \frac{1}{\sqrt{2}}(|+\rangle + |-\rangle), |O_2^+\rangle = |0\rangle, |O^-\rangle = \frac{1}{\sqrt{2}}(|+\rangle - |-\rangle)$. Therefore all eigenstates of H^{II} can't be uniquely labeled by the eigenvalues of all O_i 's as the number of such available quantum numbers (2^L) is far less than the total number of eigenstates ($\approx 2.7^L$). Thus the conserved quantities can only be used to block diagonalize the Hamiltonian. The largest block is characterized by $O_i = +1, \forall i$. It is easy to see that this sector is equivalent to the celebrated spin-1/2 PXP model with the identification $|\downarrow\rangle = |O_1^+\rangle$ and $|\uparrow\rangle = |O_2^+\rangle$. Thus, in principle one can expect to see all phenomenon observed in spin-1/2 PXP model in this spin-1 model also. On the theoretical side, Lin-Motrunich[11] type exact eigenstates can also be constructed here, not only for the largest sector but also for all sectors where island of sites with $O_i = +1$ are separated by sites with $O_i = -1$ as these sectors are nothing but disconnected patches of spin-1/2 PXP model of different sizes. The smallest sector is of size 1 with $O_i = -1$ at all sites, hence H^{II} posses an unentangled, exact zero energy eigenstates: $\prod_i |O_i^-\rangle$.

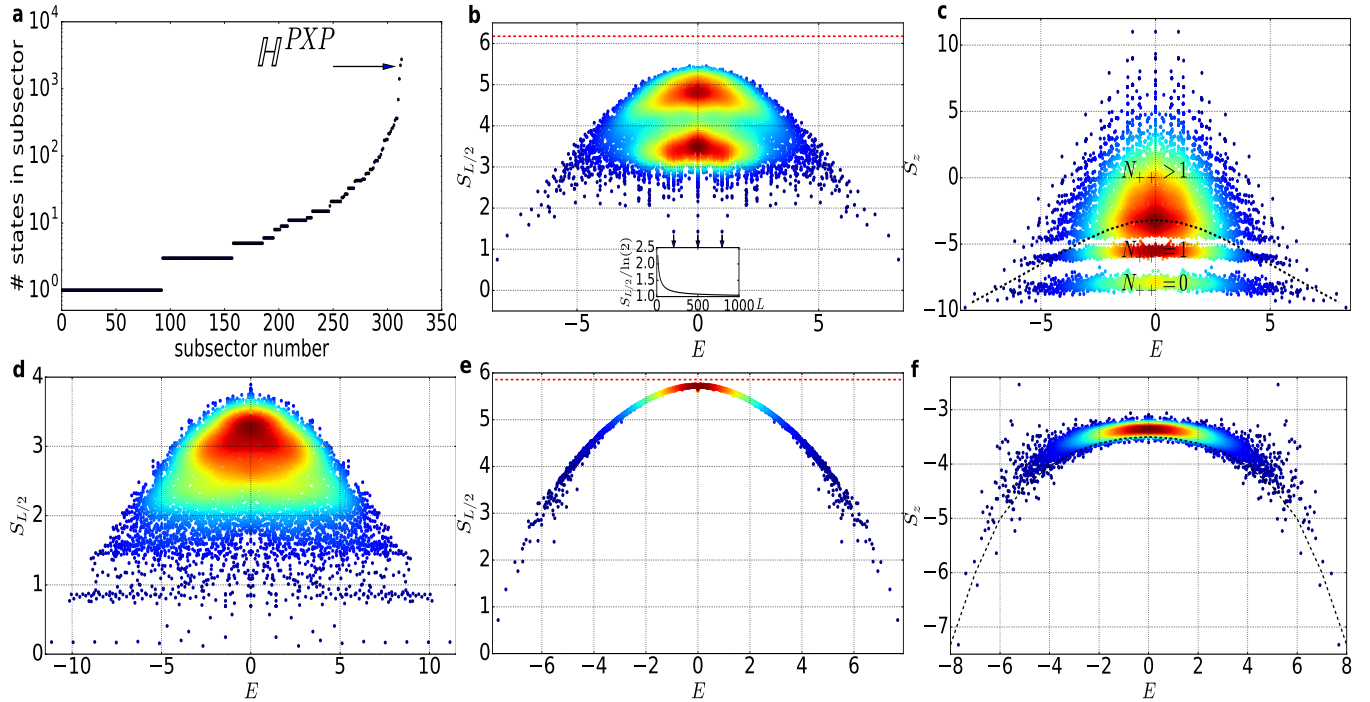


FIG. 2: Ergodicity property of Model-I, II & III. (a) Shattering of Hilbert space in Model-I. Size of different emergent subsectors in $K = 0, I = +1$ sector for $L = 16$. The traditional spin-1 PXP model is the 2nd largest sector at this system size. (b) $S_{L/2}$ of all the eigenstates in $K = 0, I = +1$ sector of Model-I for $L = 16$. System size scaling of $S_{L/2}$ for the three lowest entangled state is shown in the inset. (c) S_z of all eigenstates in $K = 0, I = +1$ sector of Model-I for $L = 16$. The three cluster of states ($n = 2, \dots, L - 2$) sites are labeled by the value of N_{++} . (d) $S_{L/2}$ of all the eigenstates of Model-II which belong to the sectors where central n ($n = 2, \dots, L - 2$) sites are labeled by $O = +1$ and the rest are $O = -1, L = 20$. (e) $S_{L/2}$ and (f) S_z of all the eigenstates in $K = 0, I = +1$ sector of Model-III, $L = 14$. In Panel (b),(e) the Page value of $S_{L/2}$ is shown in red dashed line. For panel (d) Page value ($S_{L/2}^{Page} = 9.625$) is not shown. In Panel (c) and (f) the canonical (Gibbs) ensemble prediction of S_z is shown in black dashed line.

We note that sectors where at least two consecutive sites have $O_i = +1$ feels the hardcore interaction whereas sectors where each $O_i = +1$ site is isolated by at least one $O_i = -1$ from both side is basically non-interacting in nature. The number of such non-interacting sectors scales as $\sim \phi^L$. Thus though many sectors of this model is non-integrable in nature there exist exponentially many eigenstates which violates ETH .

Model-III does not allow $|00\rangle$ and $|++\rangle$ type configurations. This model neither have any conserved quantity (other than translation, inversion and particle-hole) nor its spectrum have any emergent shattering. Due to the high connectivity in Hilbert space, this model displays strongly ergodic behavior (see Fig.2(e),(f)). In the next section we will analyze it more using FSA and \mathbb{Z}_2 -dynamics.

\mathbb{Z}_2 dynamics and FSA : The difference in ergodicity of Model-I, II & III can be probed by studying the dynamics of local observables (we choose $O = (|+\rangle\langle +|)_i \otimes (|+\rangle\langle +|)_{i+1}$) from the initial state $|\mathbb{Z}_2\rangle = \otimes_{i=1}^{L/2} |-\rangle_{2i-1} |+\rangle_{2i}$. It is worthy to point out here that all standard spin- s PXP models studied so far exhibits long lived coherent oscillation starting from the

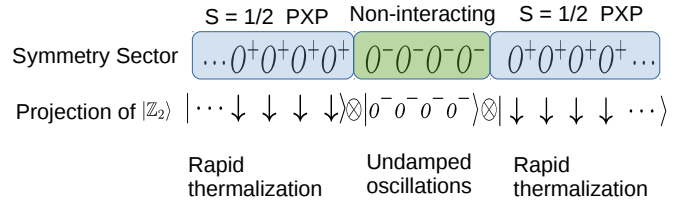


FIG. 3: Schematic structure of a typical symmetry sector of Model-II and projection of \mathbb{Z}_2 state in that sector.

\mathbb{Z}_2 state[19]. In our Model-I the \mathbb{Z}_2 state belong to the emergent subsector \mathbb{H}^{PXP} and so the corresponding dynamics will be exactly same as that of traditional spin-1 PXP model. On the other hand, $|\mathbb{Z}_2\rangle$ state has uniform overlap with all 2^L symmetry sectors of Model-II as can be seen from the expression : $|\mathbb{Z}_2\rangle = 2^{-L/2} [\otimes_{i=1}^{L/2} (|O_1^+\rangle - |O_1^-\rangle)_{2i-1} (|O_1^+\rangle + |O_1^-\rangle)_{2i}]$. Now how the state evolves inside a particular sector depends crucially on the interacting nature of that sector. The system will have perfect revival and no dephasing inside the fully non-interacting sectors whereas inside the interacting sectors it will thermalize rapidly to infinite

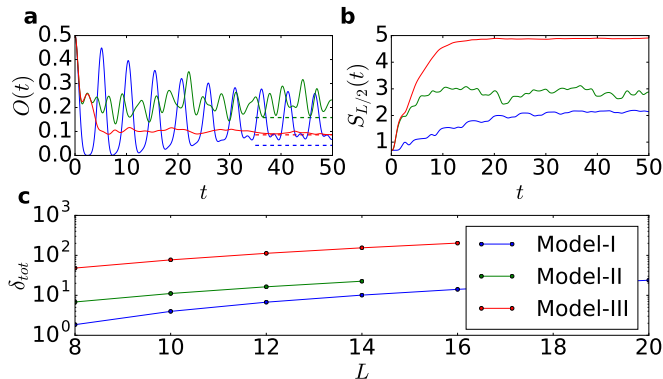


FIG. 4: (a) Dynamics of a local observable (see text) in the three models. $L = 12$ (b) Dynamics of $S_{L/2}$. $L = 12$ (c) Behavior of total FSA errors as a function of system size.

temperature (see Fig.3). This is because the projection of the initial state in the interacting sectors corresponds to the fully polarized down state ($\cdots \downarrow\downarrow\downarrow \cdots$) whereas the sectors themselves are nothing but disconnected patches of spin-1/2 PXP model of different sizes. So the \mathbb{Z}_2 -dynamics in Model-II is a mixture of maximally thermal and maximally non-thermal effects, as a result neither it shows strong coherent oscillation nor thermalizes quickly (see Fig.4(a)). We note that though the number of fully non-interacting sectors ($\sim \phi^L$) is a vanishingly small fraction ($\sim 0.81^L$) of total number of sectors in thermodynamic limit, sectors with small interacting portions also increase exponentially with system sizes. Therefore the nature of the dynamics in thermodynamic limit is an interesting open question. Finally, we find that the \mathbb{Z}_2 -dynamics in Model-III thermalizes rapidly to infinite temperature due to the strongly ergodic na-

ture of the model. We show entanglement dynamics of the three model in Fig.4 (b). The initial growth of entanglement (which is related to the speed of information propagation) is fastest in Model-III, slowest in Model-I and intermediate in Model-II. This is consistent with the nature of the dynamics of local observable in these three models.

We now corroborate our dynamics results using FSA which has been very successful in capturing the scar states in large PXP systems[9, 10]. We begin by decomposing H^α into two parts: $H^\alpha = H_+^\alpha + H_-^\alpha$ such that H_-^α annihilates the initial state $|v_0\rangle = |\mathbb{Z}_2\rangle$ and $H_+^\alpha = (H_-^\alpha)^\dagger$. The repeated application of H_+^α on $|\mathbb{Z}_2\rangle$ generates the FSA vectors $|v_n\rangle = \frac{1}{\beta_n} H_+^\alpha |v_{n-1}\rangle$. For the spin-1 models in this paper, n runs from 0 to $2L$ after which the state gets annihilated. The FSA errors quantified by $\delta_n^\alpha = \|H_-^\alpha |v_n\rangle - \beta_n |v_{n-1}\rangle\|$, $n = 1, \dots, 2L$ are a measure of damping force felt by the dynamical system due to many body interaction effects. The system exhibits undamped oscillations when all the δ_n are zero which can be seen in a free paramagnet (no constraints) or by adding suitable perturbation of appropriate strength with the constrained model [14]. Though, in general, FSA errors are non-zero in PXP type constrained systems considered here, it could be zero in first few steps depending on the nature of the constraints. For example, we find that in our Model-I, first four FSA steps are exact (i.e error free) and error arises at fifth (n_f) step. For Model-II and III error arises at 3rd and 2nd FSA step respectively. This errors cause dephasing; higher the errors, higher is the rate of dephasing. Here we give analytical expression (See [30]) of first nonzero FSA error ($\delta_{n_f}^\alpha$) for the three models

$$\begin{aligned}
 \delta_{n_f(=5)}^I &= \frac{12(L^3 - 6L^2 + 11L - 18)}{(L-1)(L-2)(L-3)(5L^4 - 50L^3 + 175L^2 - 250L + 144)} \\
 \delta_{n_f(=3)}^{II} &= \frac{50(2L-9)}{(2L-5)(6L^2 - 45L + 95)} \\
 \delta_{n_f(=2)}^{III} &= \frac{1}{4(4L-11)}
 \end{aligned} \tag{2}$$

In brief, $\delta_{n_f} \sim L^{-(n_f-1)}$ at large L , from which it is easy to see that $\delta_{n_f}^I < \delta_{n_f}^{II} < \delta_{n_f}^{III}$. We numerically calculate the FSA errors in higher steps ($n > n_f$) and plot the behavior of total FSA error ($\delta_{tot} = \sum_{n=1}^{2L} \delta_n$) in Fig.4. One can again see that $\delta_{tot}^I < \delta_{tot}^{II} < \delta_{tot}^{III}$. This gives a qualitative understanding of the hierarchy of entanglement growth, amount of oscillation present in

the dynamics of local observable and ergodicity of the models.

Conclusion & Discussion : In summary we have studied the change in ergodic properties of spin-1 PXP model for three specific choices of constraints. We find that whereas certain set of constraints can shatter the Hilbert space into exponentially many emergent subsectors, thus

leading to violation of ETH, some other set of constraints can destroy all the anomalous states and make the spectrum strongly ergodic. Our choice of constraints (only between the excited states $|0\rangle$ and $|+\rangle$ in nearest neighbor (n.n) sites) is motivated by the experimental realization of spin-1/2 PXP model in Rydberg atom systems where strong repulsive interaction between n.n atoms is turned on only when they are simultaneously in the excited (Rydberg) states[8]. A detail study of all such set of constraints is beyond the scope of the current work[20]. But we have checked that there are other set of constraints which belong to the first category (i.e in the class of Model-I). For example, if only $|+0\rangle$ and $|0+\rangle$ type of constraints are not allowed, then also the constrained Hilbert space ($d_L^{OBC} \sim 2.414^L$) gets shattered into many blocks of different sizes. In fact the special eigenstates of Model-I (with integer energies) are also the eigenstates of this Model. Note that this model differs from Model-I by only the presence of $|00\rangle$ type of configurations which means the inert sector or the special eigenstates of Model-I are robust against this change of constraints. On the experimental side, we note that non-ergodic quantum dynamics due to emergent kinetic constraint and Hilbert space fragmentation is recently observed in tilted Fermi-Hubbard model at large tilt potential[33]. Secondly, we believe that the Model-II is a minimal interacting model where non-integrability and extensive number of local conserved quantities coexist. It will be interesting to explore the existence of such models in other type of systems. Finally, the strong ergodic nature of Model-III is also remarkable because we find that quantum scars exist and ETH violation happens even when only $|++\rangle$ type of configurations are forbidden. We leave the study of detailed mechanism behind this constraint induced strong ergodicity and the exploration of class of constraints which leads to the same behavior as a future problem.

Acknowledgments : This work is supported by the Shanghai Municipal Science and Technology Major Project (Grant No. 2019SHZDZX01) [B.M., Z.C., W.V.L.], National Key Research and Development Program of China (Grants No. 2016YFA0302001 and 2020YFA0309000) and NSFC of China (Grants No. 11674221 and No. 11574200) [Z.C] and by the AFOSR Grant No. FA9550-16-1-0006 and the MURI-ARO Grant No. W911NF17-1-0323 through UCSB [W.V. L.].

* Electronic address: bhaskarmukherjee1991@gmail.com

† Electronic address: zcai@sjtu.edu.cn

‡ Electronic address: wvliu@pitt.edu

- [1] L. D'Alessio, Y. Kafri, A. Polkovnikov, M. Rigol, *Adv. Phys.* **65**, 239 (2016).
 [2] J. M. Deutsch, *Phys. Rev. A* **43**, 2046 (1991).
 [3] M. Srednicki, *Phys. Rev. E* **50**, 888 (1994); *J. Phys. A* **32**, 1163 (1999).

- [4] M. Rigol, V. Dunjko, and M. Olshanii, *Nature (London)* **452**, 854 (2008).
 [5] Sutherland, B. *Beautiful Models: 70 Years of Exactly Solved Quantum Many-body Problems* (World Scientific, River Edge, NJ, 2004).
 [6] Sachdev, Subir (1999). *Quantum phase transitions*. Cambridge University Press.
 [7] M. Basko, I. L. Aleiner, and B. L. Altshuler, *Ann. Phys.* **321**, 1126 (2006); V. Oganesyan and D. A. Huse, *Phys. Rev. B* **75**, 155111 (2007); A. Pal and D. A. Huse, *ibid.* **82**, 174411 (2010); D. A. Huse, R. Nandkishore, V. Oganesyan, A. Pal, and S. L. Sondhi, *ibid.* **88**, 014206 (2013); R. Vosk and E. Altman, *Phys. Rev. Lett.* **110**, 067204 (2013); M. Serbyn, Z. Papic, and D. A. Abanin, *ibid.* **111**, 127201 (2013); D. A. Huse, R. Nandkishore, and V. Oganesyan, *Phys. Rev. B* **90**, 174202 (2014); T. Grover, arXiv:1405.1471; M. Serbyn, Z. Papic, and D. A. Abanin, *Phys. Rev. X* **5**, 041047 (2015); K. Agarwal, S. Gopalakrishnan, M. Knap, M. Müller, and E. Demler, *Phys. Rev. Lett.* **114**, 160401 (2015); V. Khemani, S. P. Lim, D. N. Sheng, and D. A. Huse, *Phys. Rev. X* **7**, 021013 (2017).
 [8] H. Bernien, S. Schwartz, A. Keesling, H. Levine, A. Omran, H. Pichler, S. Choi, A. S. Zibrov, M. Endres, M. Greiner, V. Vuletic, and M. D. Lukin, *Nature* **551**, 579-584 (2017).
 [9] C. J. Turner, A. A. Michailidis, D. A. Abanin, M. Serbyn, Z. Papic, *Nat. Phys.* **14** 745 (2018)
 [10] C. J. Turner, A. A. Michailidis, D. A. Abanin, M. Serbyn, and Z. Papic, *Phys. Rev. B* **98**, 155134 (2018).
 [11] C-J Lin, Olexei I. Motrunich, *Phys. Rev. Lett.* **122**, 173401 (2019).
 [12] N. Shiraishi, *J. Stat. Mech.* (2019) 083103.
 [13] V Khemani, C. R. Laumann, A Chandran, *Phys. Rev. B* **99**, 161101 (2019).
 [14] S. Choi et al, *Phys. Rev. Lett.* **122**, 220603 (2019).
 [15] M. Schechter and T. Iadecola, *Phys. Rev. Lett.* **123**, 147201 (2019).
 [16] S. Moudgalya, S. Rachel, B. A. Bernevig, and N. Regnault, *Phys. Rev. B* **98**, 235155 (2018); S. Maudgalya, N. Regnault, B.A. Bernevig, *Phys. Rev. B* **98**, 235156 (2018)
 [17] D K Mark, O I Motrunich, *Phys. Rev. B* **102**, 075132 (2020); S Moudgalya, N Regnault, B A Bernevig, *Phys. Rev. B* **102**, 085140 (2020).
 [18] N. Shiraishi, T. Mori, *Phys. Rev. Lett.* **119**, 030601 (2017)
 [19] W. W. Ho, S. Choi, H. Pichler, and M. D. Lukin, *Phys. Rev. Lett.* **122**, 040603 (2019).
 [20] K. Bull, I. Martin, and Z. Papic, *Phys. Rev. Lett.* **123**, 030601 (2019).
 [21] B. Mukherjee, S. Nandy, A.Sen, D. Sen and K. Sengupta, *Phys. Rev. B* **101**, 245107 (2020) ; B. Mukherjee, A.Sen, D. Sen and K. Sengupta, *Phys. Rev. B* **102**, 014301 (2020) ; B. Mukherjee, A.Sen, D. Sen and K. Sengupta, *Phys. Rev. B* **102**, 075123 (2020) ; S. Pai and M. Pretko, *Phys. Rev. Lett.* **123**, 136401 (2019) ; S. Sugiura, T. Kuwahara, K. Saito, arXiv:1911.06092 ; K. Mizuta, K. Takasan and Norio Kawakami, *Phys. Rev. Research* **2**, 033284 (2020).
 [22] N. Shibata, N. Yoshioka, and H. Katsura, *Phys. Rev. Lett.* **124**, 180604 (2020).
 [23] S. Maudgalya, N. Regnault, B.A. Bernevig, *Phys. Rev. B* **102**, 195150 (2020).
 [24] Seulgi Ok et al, *Phys. Rev. Research* **1**, 033144 (2019),

- C-J Lin, V Calvera, T. H. Hsieh, Phys. Rev. B 101, 220304(R) (2020).
- [25] A. J. A. James, R. M. Konik, N. J. Robinson, Phys. Rev. Lett. 122, 130603 (2019).
- [26] T. Iadecola, M. Schechter, S. Xu, Phys. Rev. B 100, 184312 (2019).
- [27] D. Banerjee, A. Sen, arxiv: 2012.08540 ; V. Karle, M. Serbyn, A. A. Michailidis, arxiv : 2102.13633.
- [28] Vedika Khemani, Michael Hermele, Rahul M. Nandkishore, Phys. Rev. B 101, 174204 (2020).
- [29] P. Sala, T. Rakovszky, R. Verresen, M. Knap, and F. Pollmann, Phys. Rev. X 10, 011047 (2020).
- [30] See Supplemental material for details.
- [31] ZC Yang, F Liu, AV Gorshkov, T. Iadecola, Phys. Rev. Lett. 124, 207602 (2020).
- [32] Thomas Iadecola, Michael Schechter, Phys. Rev. B 101, 024306 (2020).
- [33] Sebastian Scherg et al, arXiv:2010.12965.

Supplemental material for “Constraint-induced breaking and restoration of ergodicity in spin-1 PXP models”

Growth of Hilbert space dimension for Model-I, II & III

The constraints leads to a slower growth of Hilbert space dimension compared to naive 3^L . Atfirst we demonstrate it for open boundary condition (OBC). We start by Model-I for which $|+0\rangle, |0+\rangle, |00\rangle$ type of configurations are not allowed. Any state in a system of size L may end by $|-\rangle, |0\rangle$ or $|+\rangle$. All states in a L site system which are ending by $|-\rangle$ can be obtained by simply appending a $|-\rangle$ to all states in a $L - 1$ site system. The states which are ending by $|0\rangle$ in a L site system can be obtained by appending $|-\rangle$ to all states in a $L - 2$ site system whereas $|+\rangle$ can only be appended if the last site is not in the state $|0\rangle$. This leads to the following recurrence relation of total number of states (d_L) in a system of size L

$$\begin{aligned} d_L &= d_L^- + d_L^0 + d_L^+ \\ &= d_{L-1} + d_{L-2} + (d_{L-1} - d_{L-3}) \\ &= 2d_{L-1} + d_{L-2} - d_{L-3} \end{aligned} \quad (3)$$

which can be cast in the following matrix form

$$\begin{pmatrix} d_L \\ d_{L-1} \\ d_{L-2} \end{pmatrix} = \begin{pmatrix} 2 & 1 & -1 \\ 1 & 0 & 0 \\ 0 & 1 & 0 \end{pmatrix} \begin{pmatrix} d_{L-1} \\ d_{L-2} \\ d_{L-3} \end{pmatrix} \quad (4)$$

The eigenvalues of this matrix are $\approx (2.247, -0.802, 0.555)$. It is difficult to get an exact expression of d_L for Model-I but the leading behavior in the large L limit will be controlled by the largest eigenvalue 2.247 (as this is the only one with magnitude > 1).

Model-II does not allow $|00\rangle$ type configurations only. So, $|0\rangle$ can only be appended if the last site is either in state $|+\rangle$ or $|-\rangle$. The recurrence relation for d_L is given by

$$\begin{aligned} d_L &= d_L^- + d_L^0 + d_L^+ \\ &= d_{L-1} + (d_{L-1}^+ + d_{L-1}^-) + d_{L-1} \\ &= 2d_{L-1} + 2d_{L-2} \end{aligned} \quad (5)$$

which can be cast in the following matrix form

$$\begin{pmatrix} d_L \\ d_{L-1} \end{pmatrix} = \begin{pmatrix} 2 & 2 \\ 1 & 0 \end{pmatrix} \begin{pmatrix} d_{L-1} \\ d_{L-2} \end{pmatrix} = \begin{pmatrix} 2 & 2 \\ 1 & 0 \end{pmatrix}^{L-2} \begin{pmatrix} d_2 \\ d_1 \end{pmatrix} \quad (6)$$

using $d_1 = 3$ and $d_2 = 8$ one get the expression of d_L as a function of L (see Table-I in main text).

In Model-III $|+0\rangle/|0+\rangle$ type of configurations are not allowed. States which are ending by $|0\rangle(|+\rangle)$ in a L site system can be obtained by appending $|0\rangle(|+\rangle)$ to all states of a $L - 1$ site system which are not ending by $|+\rangle(|0\rangle)$. Therefore,

$$\begin{aligned} d_L &= d_L^- + d_L^0 + d_L^+ \\ &= d_{L-1} + (d_{L-1} - d_{L-1}^+) + (d_{L-1} - d_{L-1}^0) \\ &= 3d_{L-1} - (d_{L-1}^0 + d_{L-1}^+) \\ &= 2d_{L-1} + d_{L-2} \end{aligned} \quad (7)$$

this recurrence relation can be represented in the following matrix form

$$\begin{pmatrix} d_L \\ d_{L-1} \end{pmatrix} = \begin{pmatrix} 2 & 1 \\ 1 & 0 \end{pmatrix} \begin{pmatrix} d_{L-1} \\ d_{L-2} \end{pmatrix} = \begin{pmatrix} 2 & 1 \\ 1 & 0 \end{pmatrix}^{L-2} \begin{pmatrix} d_2 \\ d_1 \end{pmatrix} \quad (8)$$

the exact expression of d_L for Model-I can be calculated using $d_1 = 3$ and $d_2 = 7$ (see Table-I in main text).

Hilbert space dimension in *PBC* will be somewhat smaller than the corresponding number in *OBC* as some of the configurations(which does not satisfies the constraints between the two end spins) will be eliminated.

Special states of Model-I and their properties

Inert states

There are exponentially many states inside the constrained Hilbert space of Model-I that are not connected by the Hamiltonian with other states and hence inert [13, 29]. Inert states are unentangled, zero-energy eigenstates of H^I . We first consider the most obvious one : $|+++\dots\rangle$, the product of $|S_z = 1\rangle$ state at all sites. Starting from this state, one can construct other inert states by inserting one or more $|-\rangle$ in the sea of $|+\rangle$ states. There can not be three consecutive $|-\rangle$ state and isolated (i.e surrounded by at least one $|-\rangle$ from both side) $|+\rangle$ state, as the presence of such configurations makes the state active. Note that, due to the same reason, presence of any $|0\rangle$ state is also not allowed. We find that the exact number of inert states (I_L) for system size L follows the recurrence relation $I_L = I_{L-1} + I_{L-3} + I_{L-4}$ which can be cast in the following matrix form

$$\begin{pmatrix} I_L \\ I_{L-1} \\ I_{L-2} \\ I_{L-3} \end{pmatrix} = \begin{pmatrix} 1 & 0 & 1 & 1 \\ 1 & 0 & 0 & 0 \\ 0 & 1 & 0 & 0 \\ 0 & 0 & 1 & 0 \end{pmatrix} \begin{pmatrix} I_{L-1} \\ I_{L-2} \\ I_{L-3} \\ I_{L-4} \end{pmatrix} \quad (9)$$

Interestingly this holds for both *PBC* and *OBC*. Therefore, raising this matrix to appropriate power and using suitable boundary conditions we get

$$\begin{aligned} I_L^{OBC} &= \frac{1}{10}((3 + \sqrt{5})\phi^L - (3 - \sqrt{5})\left(\frac{-1}{\phi}\right)^L + 4(\cos(\frac{\pi L}{2}) - 2\sin(\frac{\pi L}{2}))) \\ I_L^{PBC} &= 2\cos(\frac{\pi L}{2}) + \phi^L + \phi^{-L} \end{aligned} \quad (10)$$

where $\phi(= \frac{1+\sqrt{5}}{2})$ is the Fibonacci number. It is easy to see that for large systems $I_L \sim c\phi^L$ where $c = 1(0.523)$ for *PBC*(*OBC*) which means there is nearly half amount of inert states in *OBC* compared to *PBC*.

Special states with integer energies

Special states with energy $E = \pm 1$ are given by

$$|\psi_{\pm 1}\rangle = \frac{1}{2}|\psi_{-}\rangle + \frac{1}{2}|\psi_{+}\rangle \pm \frac{1}{\sqrt{2}}|\psi_0\rangle \quad (11)$$

where

$$\begin{aligned} |\psi_{-}\rangle &= \frac{1}{\sqrt{L}} \sum_{n=1}^L T^n \underbrace{|+\dots+\rangle}_{L-3} |-\rangle \\ |\psi_{+}\rangle &= \frac{1}{\sqrt{L}} \sum_{n=1}^L T^n \underbrace{|+\dots+\rangle}_{L-3} |-\rangle \\ |\psi_0\rangle &= \frac{1}{\sqrt{L}} \sum_{n=1}^L T^n \underbrace{|+\dots+\rangle}_{L-3} |0\rangle \end{aligned} \quad (12)$$

Next, eigenstates with energy $E = \pm 2$ are given by

$$|\psi_{\pm 2}\rangle = \pm \frac{1}{4}|\psi_{--}\rangle \pm \frac{1}{\sqrt{8}}|\psi_{+-}\rangle \pm \frac{1}{4}|\psi_{++}\rangle + \frac{1}{2}|\psi_{0-}\rangle + \frac{1}{2}|\psi_{+0}\rangle \pm \frac{1}{2}|\psi_{00}\rangle \quad (13)$$

where

$$\begin{aligned} |\psi_{--}\rangle &= \sqrt{\frac{2}{L}} \sum_{n=1}^{L/2} T^n |\underbrace{+\cdots+}_{\frac{L}{2}-3} - \underbrace{+\cdots+}_{\frac{L}{2}-3} -\rangle \\ |\psi_{+-}\rangle &= \frac{1}{\sqrt{L}} \sum_{n=1}^L T^n |\underbrace{+\cdots+}_{\frac{L}{2}-3} + \underbrace{+\cdots+}_{\frac{L}{2}-3} -\rangle \\ |\psi_{++}\rangle &= \sqrt{\frac{2}{L}} \sum_{n=1}^{L/2} T^n |\underbrace{+\cdots+}_{\frac{L}{2}-3} + \underbrace{+\cdots+}_{\frac{L}{2}-3} +\rangle \\ |\psi_{0-}\rangle &= \frac{1}{\sqrt{L}} \sum_{n=1}^L T^n |\underbrace{+\cdots+}_{\frac{L}{2}-3} - \mathbf{0} - \underbrace{+\cdots+}_{\frac{L}{2}-3} -\rangle \\ |\psi_{+0}\rangle &= \frac{1}{\sqrt{L}} \sum_{n=1}^L T^n |\underbrace{+\cdots+}_{\frac{L}{2}-3} + \underbrace{+\cdots+}_{\frac{L}{2}-3} - \mathbf{0} -\rangle \\ |\psi_{00}\rangle &= \sqrt{\frac{2}{L}} \sum_{n=1}^{L/2} T^n |\underbrace{+\cdots+}_{\frac{L}{2}-3} - \mathbf{0} - \underbrace{+\cdots+}_{\frac{L}{2}-3} - \mathbf{0} -\rangle \end{aligned} \quad (14)$$

Red (blue) colored sites are inert (active). Note that there is a structural resemblance between the states in Eq.(11),(12) and in Eq.(13),(14). The later type of states (in a system of size L) is obtained by a spatial addition of different combinations of the former type of states (in a system of size $L/2$). This also explains the additivity of their energies.

Proof of eigenstates

Here we prove that the special states in Eq. (11), (13) are exact eigenstates of Model-I. We find that the following relations hold for the states in Eq. (12) and Model-I.

$$\begin{aligned} H^I |\psi_{-}\rangle &= \frac{1}{\sqrt{2}} |\psi_0\rangle \\ H^I |\psi_{+}\rangle &= \frac{1}{\sqrt{2}} |\psi_0\rangle \\ H^I |\psi_0\rangle &= \frac{1}{\sqrt{2}} (|\psi_{+}\rangle + |\psi_{-}\rangle) \end{aligned} \quad (15)$$

These relations together gives $H^I |\psi_{\pm 1}\rangle = \pm |\psi_{\pm 1}\rangle$

Similarly for the states in Eq. (14), we find

$$\begin{aligned}
H^I|\psi_{--}\rangle &= |\psi_{0-}\rangle \\
H^I|\psi_{+-}\rangle &= \frac{1}{\sqrt{2}}(|\psi_{0-}\rangle + |\psi_{+0}\rangle) \\
H^I|\psi_{++}\rangle &= |\psi_{+0}\rangle \\
H^I|\psi_{0-}\rangle &= |\psi_{--}\rangle + |\psi_{00}\rangle + \frac{1}{\sqrt{2}}|\psi_{+-}\rangle \\
H^I|\psi_{+0}\rangle &= \frac{1}{\sqrt{2}}|\psi_{+-}\rangle + |\psi_{++}\rangle + |\psi_{00}\rangle \\
H^I|\psi_{00}\rangle &= |\psi_{0-}\rangle + |\psi_{+0}\rangle
\end{aligned} \tag{16}$$

These relations together gives $H^I|\psi_{\pm 2}\rangle = \pm 2|\psi_{\pm 2}\rangle$.

Magnetization

Here we show that the special eigenstates have integer magnetization ($S_z = \sum_i S_i^z$).

For states in Eq.(11)

$$\langle\psi_{\pm 1}|S_z|\psi_{\pm 1}\rangle = \frac{L-6}{4} + \frac{L-4}{4} + \frac{L-5}{2} = L-5 \tag{17}$$

For states in Eq.(13)

$$\langle\psi_{\pm 2}|S_z|\psi_{\pm 2}\rangle = \frac{L-12}{16} + \frac{L-10}{8} + \frac{L-8}{16} + \frac{L-11}{4} + \frac{L-9}{4} + \frac{L-10}{4} = L-10 \tag{18}$$

Similarly for states with energy $E = \pm n$, magnetization will be $L - 5n$. We note that there are lots of eigenstates at integer energies in Model-I. The specialty of integer energy eigenstates (e.g in (11),(13)) studied in this work is that they have minimum entanglement entropy and maximum magnetization in the corresponding manifold of states.

Entanglement entropies

The entanglement of a state can be quantified using various schemes. We use Von-Neumann formula which works in the following way : first divide the full system AB into two parts, A and B . Then the entropy of entanglement of part A with part B is given by $S_A = -Tr[\rho_A \ln(\rho_A)]$ where $\rho_A = Tr_B[\rho_{AB}]$ is the reduced density matrix of part A and ρ_{AB} is the density matrix corresponding to the state of the full system. The size of A and B can be anywhere in between 1 and $L - 1$ with the constraint $L_A + L_B = L$. As we use PBC for all our calculation, the full system AB will be in PBC we have to treat the individual part A and B using OBC . One needs to be careful while taking the partial trace of the full density matrix (to ensure $Tr[\rho_A] = 1$) as due to the constraints in Hilbert space, the state of AB is not tensor product of states in A and B (see Fig.5).

We first derive the single site reduced density matrices (ρ_1) for the special states in Eq.(11). The local HSD per site is 3, so ρ_1 is a 3×3 matrix, whose diagonal elements for the states in Eq.(11) are

$$\begin{aligned}
\rho_1^{++} &= \frac{1}{4} \cdot \frac{1}{L} \cdot (L-3) + \frac{1}{4} \cdot \frac{1}{L} \cdot (L-2) + \frac{1}{2} \cdot \frac{1}{L} \cdot (L-3) \\
&= 1 - \frac{11}{4L} \\
\rho_1^{00} &= \frac{1}{2} \cdot \frac{1}{L} \\
\rho_1^{--} &= \frac{1}{4} \cdot \frac{1}{L} \cdot 3 + \frac{1}{4} \cdot \frac{1}{L} \cdot 2 + \frac{1}{2} \cdot \frac{1}{L} \cdot 2 = \frac{9}{4L}
\end{aligned} \tag{19}$$

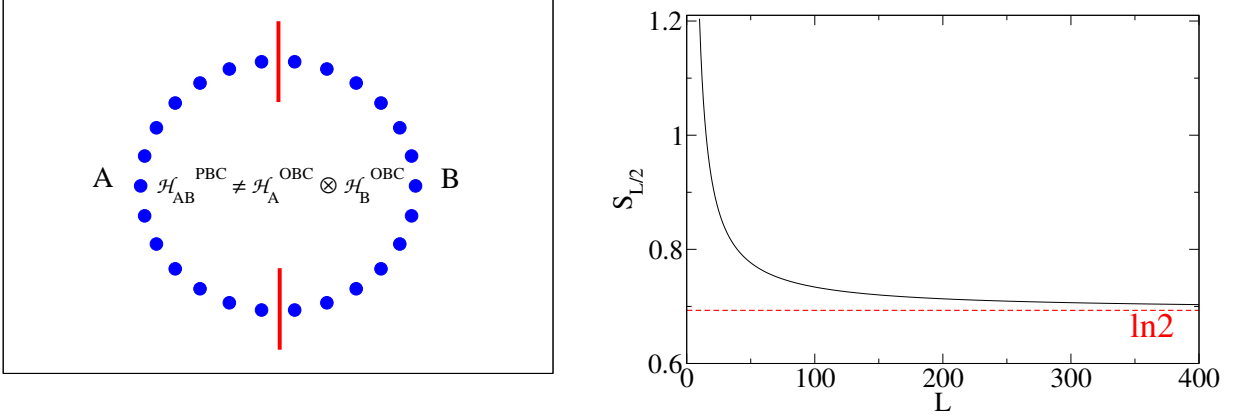


FIG. 5: left : Partition of a constrained system into two parts. right : $S_{L/2}$ as a function of L for the states in (11)

The off-diagonal elements are

$$\begin{aligned}
 \rho_1^{+0} &= \rho_1^{0+} = \frac{1}{2} \cdot \frac{1}{\sqrt{2}} \cdot \frac{1}{L} \\
 \rho_1^{+-} &= \rho_1^{-+} = \frac{1}{2} \cdot \frac{1}{2} \cdot \frac{1}{L} \\
 \rho_1^{0-} &= \rho_1^{-0} = \frac{1}{2} \cdot \frac{1}{\sqrt{2}} \cdot \frac{1}{L}
 \end{aligned} \tag{20}$$

note that all matrix elements except one diagonal element die out in the thermodynamic limit which means $\lim_{L \rightarrow \infty} S_1 = 0$. Therefore, in the thermodynamic limit, any site is unentangled with the rest of the system. This holds for the state in Eq.(13) also.

Now we concentrate on half chain entanglement entropy. Though the dimension of the corresponding reduced density matrices ($\rho_{L/2}$) scales as $\approx 2.249^{L/2}$, for the states in Eq.(11) we find only six eigenvalues are nonzero at any system size L , which are $\frac{L-4}{2L}$ (multiplicity 2) and $\frac{1}{L}$ (multiplicity 4). This gives $S_{L/2} = -2 \cdot \frac{L-4}{2L} \ln(\frac{L-4}{2L}) - 4 \cdot \frac{1}{L} \ln(\frac{1}{L})$ which has been plotted in Fig. 5. The decrease of $S_{L/2}$ with L and its saturation to the area law value ($\ln 2$) in asymptotically large system size is an artifact of the non-tensorproduct structure of the constrained Hilbert space. For the states in Eq.(13) we find the number of nonzero eigenvalues to be $L/2$ which are all equal with magnitude $\frac{2}{L}$. This gives $S_{L/2} = \frac{L}{2} \cdot \frac{2}{L} \cdot \ln(\frac{2}{L}) = \ln(L) - \ln(2)$.

Conserved quantities of Model-II

Here we show that the operators O_i commutes with the Hamiltonian H^{II} . We expand the relevant portion of H^{II}

$$\begin{aligned}
 &\mathcal{P}_{i-1,i}^{II} S_i^x \mathcal{P}_{i,i+1}^{II} \\
 &= \mathbb{I}_{i-1} \otimes S_i^x \otimes \mathbb{I}_{i+1} - \frac{1}{\sqrt{2}} \mathbb{I}_{i-1} \otimes (|+\rangle\langle 0| + |-\rangle\langle 0|)_i \otimes (|0\rangle\langle 0|)_{i+1} - \frac{1}{\sqrt{2}} (|0\rangle\langle 0|)_{i-1} \otimes (|0\rangle\langle +| + |0\rangle\langle -|)_i \otimes \mathbb{I}_{i+1}
 \end{aligned} \tag{21}$$

where we have used that $S_i^x = \frac{1}{\sqrt{2}}(|+\rangle\langle 0| + |0\rangle\langle +| + |0\rangle\langle -| + |-\rangle\langle 0|)_i$ and $\mathcal{P}_{i,i+1}^{II} = \mathbb{I}_i \otimes \mathbb{I}_{i+1} - (|0\rangle\langle 0|)_i \otimes (|0\rangle\langle 0|)_{i+1}$. It is easy to see that each part of Eq.(21) individually commutes with $O_i (= |+\rangle\langle -| + |0\rangle\langle 0| + |-\rangle\langle +|)$. Hence, $[H^{II}, O_i] = 0, \forall i$.

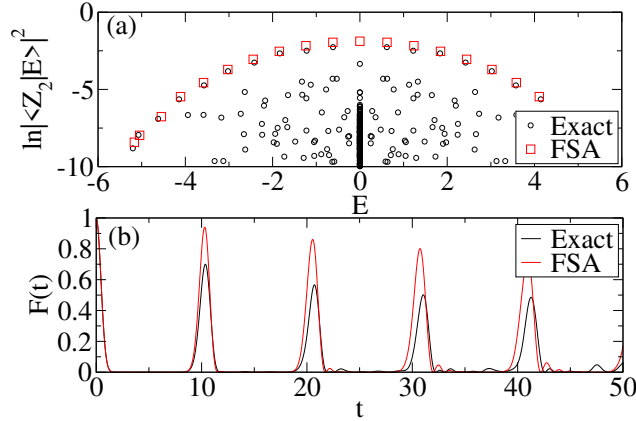


FIG. 6: Comparison of FSA with exact numerics for Model-I (a) \mathbb{Z}_2 -overlap (b) Fidelity dynamics of the \mathbb{Z}_2 state. $L=10$.

Forward Scattering Approximation

Forward scattering approximation (FSA) has been an important tool to analyze the scar induced oscillation since its first usage in spin-1/2 PXP model[9]. Here we will apply FSA in detail in our spin-1 models [20]. The essential idea is to first break the model Hamiltonians in H^+ and H^- (one is conjugate transpose to other) such that one (lets say H^-) annihilate the state $|\mathbb{Z}_2\rangle$ and the other (H^+) annihilate $|\bar{\mathbb{Z}}_2\rangle$. One state ($|\bar{\mathbb{Z}}_2\rangle / |\mathbb{Z}_2\rangle$) can be obtained from the other ($|\mathbb{Z}_2\rangle / |\bar{\mathbb{Z}}_2\rangle$) by repeated action ($2L$ times) of (H^+ / H^-). The oscillatory dynamics then can be visualized as a coherent forward and backward scattering in between these two states.

We define the n 'th FSA vector ($|v_n\rangle$) by $|v_n\rangle = \frac{1}{\beta_n} H^+ |v_{n-1}\rangle$ where $|v_0\rangle = |\mathbb{Z}_2\rangle$ and β_n is the normalization constant. Due to the choice of the initial state and structure of the Hamiltonian, FSA vectors form a closed orthonormal subspace of dimension $2L + 1$. Representation of the Hamiltonian in this subspace forms a tridiagonal matrix : $H_{FSA} = \beta_n \sum_{n=1}^{2L} |v_n\rangle\langle v_{n+1}| + h.c.$ Thus, if one is interested only in the scar subspace, an enormous simplification can be achieved, namely, one need to diagonalize a matrix whose dimension scales only linearly with system size. This enables to deal with larger system size. In Fig. 6 we have compared the \mathbb{Z}_2 -overlap of the eigenstates of H_{FSA} and fidelity dynamics of the \mathbb{Z}_2 state generated by H_{FSA} with the same quantities obtained by the full Hamiltonian (H^I) for Model-I. To calculate other quantities (e.g. some observables, entanglement entropy etc) one needs to store the FSA vectors which again consumes exponential memory (though this scales as $\sim Le^L$ but not as $\sim e^{2L}$). The mismatch of the FSA results with exact numerics in Fig. 6 is due to the fact that the FSA vectors does not form a complete set and hence can't span the Hilbert space, that's why the leakage of the \mathbb{Z}_2 dynamics out of the scar (/FSA) manifold is inevitable. This causes the revival amplitude to decrease and dephase the dynamics. This can be quantified using the FSA errors : $\delta_n = \|H^- |v_n\rangle - \beta_n |v_{n-1}\rangle\|$. If the action of H^- on a FSA vector completely undo the action of H^+ on the same vector, δ is zero and the corresponding FSA step is exact. In an ideal paramagnet (described by $H = \sum_i S_i^x$) all FSA steps are exact but due to the constraints induced by the projectors, FSA errors are nonzero in PXP models. Interestingly suitable term can be added to the bare PXP model which can reduce[21] the FSA errors even to zero[14]. In this situation the \mathbb{Z}_2 dynamics remains totally confined in the scar manifold which results in an undamped oscillation up to very long time. This suggests that the FSA errors produces some kind of frictional force in the system and hence the amplitude of oscillation (/degree of fidelity revival) should be inversely proportional to the total (summed over all the FSA steps) amount of FSA errors present in the system. Motivated by these arguments, we plan to perform a detail analysis of the FSA errors for Model-I-III.

FSA for Model-I

In Model-I $|00\rangle, |1+0\rangle, |0+\rangle$ type of configurations are not allowed. We start with

$$H_I^+|v_0\rangle = \frac{1}{\sqrt{2}} \sum_{i \text{ even}} |\cdots 0_i \cdots\rangle \quad (22)$$

where \cdots represents sea of repeated $+ - / - +$ configurations (with a suitably added $+$ or $-$ at the end). So, $\beta_1 = \sqrt{\|H_I^+|v_0\rangle\|} = \sqrt{L}/2$.

$$|v_1\rangle = \frac{1}{\beta_1} H_I^+|v_0\rangle = \sqrt{\frac{2}{L}} \sum_{i \text{ even}} |\cdots 0_i \cdots\rangle \quad (23)$$

One can easily check : $H_I^-|v_1\rangle = \beta_1|v_0\rangle$. Therefore, $\delta_1^I = 0$.

Next,

$$H_I^+|v_1\rangle = \frac{1}{\sqrt{L}} \left(\sum_{i \text{ even}} |\cdots - \frac{-}{i} - \cdots\rangle + 2 \sum_{\substack{i,j \text{ even} \\ i \neq j}} |\cdots 0_i \cdots 0_j \cdots\rangle \right) \quad (24)$$

There are $\frac{L}{4}(\frac{L}{2} - 1)$ distinct 2nd type of states. The 2nd summation should be understood as a sum over only this many number of states (that's why we bring a factor 2 before it). All such summation notations in this paper avoid double counting. We get, $\beta_2 = \sqrt{\|H_I^+|v_1\rangle\|} = \sqrt{\frac{1}{L} \cdot \frac{L}{2} + \frac{4}{L} \cdot \frac{L}{4} \cdot (\frac{L}{2} - 1)} = \frac{\sqrt{L-1}}{\sqrt{2}}$. and $|v_2\rangle = \frac{1}{\beta_2} H_I^+|v_1\rangle$. It is easy to see that $H_I^-|v_2\rangle = \beta_2|v_1\rangle$. $\therefore \delta_2^I = 0$.

Next we find

$$H_I^+|v_2\rangle = \sqrt{\frac{1}{L(L-1)}} \left(3 \sum_{\substack{i,j \text{ even} \\ i \neq j}} |\cdots 0_i \cdots - \frac{-}{j} - \cdots\rangle + 6 \sum_{\substack{i,j,k \text{ even} \\ i \neq j \neq k}} |\cdots 0_i \cdots 0_j \cdots 0_k \cdots\rangle \right) \quad (25)$$

the number of distinct 2nd type of states is $\frac{1}{3!} \frac{L}{2} (\frac{L}{2} - 1) (\frac{L}{2} - 2) = \frac{L(L-2)(L-4)}{48}$. Therefore, $\beta_3^2 = \frac{1}{L(L-1)} (9 \cdot \frac{L}{2} \cdot (\frac{L}{2} - 1) + 36 \cdot \frac{L(L-2)(L-4)}{48}) = \frac{3(L-2)}{4}$. $|v_3\rangle = \frac{1}{\beta_3} H_I^+|v_2\rangle$ and we again find $H_I^-|v_3\rangle = \beta_3|v_2\rangle$ which means $\delta_3^I = 0$.

Next we find

$$H_I^+|v_3\rangle = \frac{\sqrt{2}}{\sqrt{3L(L-1)(L-2)}} \left(3 \sum_{\substack{i,j \text{ even} \\ i \neq j}} |\cdots - \frac{-}{i} - \cdots\rangle + 12 \sum_{\substack{i,j,k \text{ even} \\ i \neq j \neq k}} |\cdots 0_i \cdots 0_j \cdots - \frac{-}{k} - \cdots\rangle + 24 \sum_{\substack{i,j,k,l \text{ even} \\ i \neq j \neq k \neq l}} |\cdots 0_i \cdots 0_j \cdots 0_k \cdots 0_l \cdots\rangle \right) \quad (26)$$

Therefore, $\beta_4^2 = \|H_I^+|v_3\rangle\| = \frac{2}{3L(L-1)(L-2)} (36 \cdot \frac{L}{4} (\frac{L}{2} - 1) + 144 \cdot \frac{L(L-2)(L-4)}{16} + 576 \cdot \frac{L(L-2)(L-4)(L-6)}{384}) = L - 3$ where we have used the fact that the number of distinct 2nd and 3rd type of states in Eq.(26) are $\frac{L(L-2)(L-4)}{16}$ and $\frac{L(L-2)(L-4)(L-6)}{384}$ respectively. $|v_4\rangle = \frac{1}{\beta_4} H_I^+|v_3\rangle$ and one can again check $\delta_4^I = 0$. Note that the first part of H_I^+ (i.e $\sum_{i \text{ odd}} \sigma_i^+$) has null effect till now.

Finally we arrive at the 5th step where non-zero FSA error arises for the first time. Calculations of FSA vectors become cumbersome from this step onward as both part of H_I^+ will now have non-zero actions. After regrouping all similar type of states we write a consolidated expression of the action of H_I^+ on $|v_4\rangle$

$$H_I^+|v_4\rangle = \frac{1}{\sqrt{3L(L-1)(L-2)(L-3)}} \left(30 \sum_{\substack{i,j,k \text{ even} \\ i \neq j \neq k}} |\cdots 0_i \cdots - \frac{-}{j} - \cdots - \frac{-}{k} - \cdots\rangle + 6 \sum_{i \text{ odd}} |\cdots - \frac{-}{i} - \cdots\rangle + 60 \sum_{\substack{i,j,k,l \text{ even} \\ i \neq j \neq k \neq l}} |\cdots 0_i \cdots 0_j \cdots 0_k \cdots - \frac{-}{l} - \cdots\rangle + 120 \sum_{\substack{i,j,k,l,m \text{ even} \\ i \neq j \neq k \neq l \neq m}} |\cdots 0_i \cdots 0_j \cdots 0_k \cdots 0_l \cdots 0_m \cdots\rangle \right) \quad (27)$$

Counting the respective number of different states in Eq.(27) we get

$$\begin{aligned}
\beta_5^2 &= \|H_I^+|v_4\rangle\| \\
&= \frac{1}{3L(L-1)(L-2)(L-3)} \left[30^2 \cdot \frac{L(L-2)(L-4)}{16} + 36 \cdot \frac{L}{2} + 60^2 \cdot \frac{L(L-2)(L-4)(L-6)}{96} \right. \\
&\quad \left. + 120^2 \cdot \frac{L(L-2)(L-4)(L-6)(L-8)}{3840} \right] \\
&= \frac{5L^4 - 50L^3 + 175L^2 - 250L + 144}{4(L-1)(L-2)(L-3)}
\end{aligned} \tag{28}$$

The action of H_I^- on $|v_5\rangle (= \frac{1}{\beta_5} H_I^+|v_4\rangle)$ gives after grouping same type of states together

$$\begin{aligned}
H_I^-|v_5\rangle &= \frac{1}{\beta_5 \sqrt{6L(L-1)(L-2)(L-3)}} \left[15(L-4) \sum_{\substack{i,j \text{ even} \\ i \neq j}} |\cdots - \frac{\cdot}{i} - + \cdots - \frac{\cdot}{j} - \cdots\rangle + \right. \\
&\quad (15L-54) \sum_{i \text{ odd}} |\cdots - \frac{\cdot}{i} - - \cdots\rangle + 30(L-4) \sum_{\substack{i,j,k \text{ even} \\ i \neq j \neq k}} |\cdots 0 \cdots 0 \cdots - \frac{\cdot}{k} - \cdots\rangle + \\
&\quad \left. 60(L-4) \sum_{\substack{i,j,k,l \text{ even} \\ i \neq j \neq k \neq l}} |\cdots 0 \cdots 0 \cdots 0 \cdots 0 \cdots\rangle \right]
\end{aligned} \tag{29}$$

note that the 1st and 2nd type of states in Eq.(29) had same strength in $|v_4\rangle$ which is sufficient to see that $H_I^-|v_5\rangle$ is not proportional to $|v_4\rangle$. Thus finally error arises in 5th FSA step which can be easily calculated by evaluating the norm : $\delta_5^I = \|H_I^-|v_5\rangle - \beta_5|v_4\rangle\| = \frac{12(L^3-6L^2+11L-18)}{(L-1)(L-2)(L-3)(5L^4-50L^3+175L^2-250L+144)}$.

FSA for Model-II

Only $|00\rangle$ type of configurations are not allowed in Model-II. We start by

$$H_{II}^+|\mathbb{Z}_2\rangle = \frac{1}{\sqrt{2}} \left(\sum_{i \text{ even}} |\cdots - 0 \cdots\rangle + \sum_{i \text{ odd}} |\cdots - + 0 \cdots\rangle \right) \tag{30}$$

So $\beta_1 = \sqrt{\|H_{II}^+|\mathbb{Z}_2\rangle\|} = \sqrt{L/2}$ and $|v_1\rangle = \frac{1}{\beta_1} H_{II}^+|\mathbb{Z}_2\rangle$. It is easy to see that $H_{II}^-|v_1\rangle = \beta_1|\mathbb{Z}_2\rangle$ and hence $\delta_1^{II} = 0$. Next,

$$\begin{aligned}
H_{II}^+|v_1\rangle &= \frac{1}{\sqrt{2L}} \left[\sum_{i \text{ even}} |\cdots - \frac{\cdot}{i} - \cdots\rangle + 2 \sum_{\substack{i,j \text{ even} \\ i \neq j}} |\cdots - 0 \cdots - 0 \cdots\rangle + 2 \sum_{\substack{i \text{ even} \\ j \text{ odd}}} |\cdots - 0 \cdots + 0 \cdots\rangle + \right. \\
&\quad \left. 2 \sum_{\substack{i,j \text{ odd} \\ i \neq j}} |\cdots + 0 \cdots + 0 \cdots\rangle + \sum_{i \text{ odd}} |\cdots + \frac{\cdot}{i} + \cdots\rangle \right]
\end{aligned} \tag{31}$$

We get $\beta_2^2 = \|H_{II}^+|v_1\rangle\| = \frac{2L-5}{2}$ and $|v_2\rangle = \frac{1}{\beta_2}H_{II}^+|v_1\rangle$. It is easy to check that $H_{II}^-|v_2\rangle = \beta_2|v_1\rangle$ which means $\delta_2^{II} = 0$. Rarity of constraints produces a large number of states in the next step, we write the consolidated expression

$$\begin{aligned}
H_{II}^+|v_2\rangle = & \frac{1}{\sqrt{2L(2L-5)}} [3 \sum_{\substack{i \text{ even} \\ j \text{ odd}}} |\cdots - \frac{-}{i} - \cdots + \frac{0}{j} + \cdots\rangle + \sum_{i \text{ even}} (|\cdots - \frac{-}{i} 0 \cdots\rangle + |\cdots 0 \frac{-}{i} - \cdots\rangle) + \\
& 3 \sum_{i,j \text{ even}} |\cdots - \frac{-}{i} - \cdots - \frac{0}{j} - \cdots\rangle + 3 \sum_{i,j \text{ odd}} |\cdots + \frac{+}{i} + \cdots + \frac{0}{j} + \cdots\rangle + \sum_{i \text{ even}} (|\cdots + \frac{+}{i} 0 \cdots\rangle + |\cdots 0 \frac{+}{i} + \cdots\rangle) \\
& 3 \sum_{\substack{i \text{ even} \\ j \text{ odd}}} |\cdots - \frac{0}{i} - \cdots + \frac{+}{j} + \cdots\rangle + 6 \sum_{\substack{i,j,k \text{ even} \\ i \neq j \neq k}} |\cdots - \frac{0}{i} - \cdots - \frac{0}{j} - \cdots - \frac{0}{k} - \cdots\rangle + \\
& 6 \sum_{\substack{i,j,k \text{ odd} \\ i \neq j \neq k}} |\cdots + \frac{0}{i} + \cdots + \frac{0}{j} + \cdots + \frac{0}{k} + \cdots\rangle + 6 \sum_{\substack{i,j \text{ even} \\ k \text{ odd}}} |\cdots - \frac{0}{i} - \cdots - \frac{0}{j} - \cdots + \frac{0}{k} + \cdots\rangle \\
& 6 \sum_{\substack{i,j \text{ odd} \\ k \text{ even}}} |\cdots + \frac{0}{i} + \cdots + \frac{0}{j} + \cdots - \frac{0}{k} - \cdots\rangle] \tag{32}
\end{aligned}$$

by carefully counting the number of each type of states in Eq.(32) we find

$$\beta_3^2 = \frac{1}{2L(2L-5)} [2 \cdot (9 \cdot \frac{L}{2} \cdot (\frac{L}{2} - 2) + L + 9 \cdot \frac{L}{2} \cdot (\frac{L}{2} - 2)) + 2 \cdot (36 \cdot \frac{L(L-2)(L-4)}{48} + 36 \cdot \frac{L(L-4)(L-6)}{16})] = \frac{6L^2 - 45L + 95}{4L - 10} \tag{33}$$

and $|v_3\rangle = \frac{1}{\beta_3}H_{II}^+|v_2\rangle$. We now calculate $H_{II}^-|v_3\rangle$

$$\begin{aligned}
H_{II}^-|v_3\rangle = & \frac{1}{\sqrt{2}} \cdot \frac{1}{\sqrt{2L(2L-5)}} \cdot \frac{1}{\beta_3} [(3 \cdot (\frac{L}{2} - 2) + 2 + 3 \cdot (\frac{L}{2} - 1)) (\sum_{i \text{ even}} |\cdots - \frac{-}{i} - \cdots\rangle + \sum_{i \text{ odd}} |\cdots + \frac{+}{i} + \cdots\rangle) + \\
& (6 + 6 \cdot \frac{L-6}{2} + 6 \cdot \frac{L-6}{2}) \sum_{\substack{i \text{ even} \\ j \text{ odd}}} |\cdots - \frac{0}{i} - \cdots + \frac{0}{j} + \cdots\rangle + \\
& (6 + 6 \cdot \frac{L-4}{2} + 6 \cdot \frac{L-8}{2}) (\sum_{i,j \text{ even}} |\cdots - \frac{0}{i} - \cdots + - + \cdots - \frac{0}{j} - \cdots\rangle + \sum_{i,j \text{ odd}} |\cdots + \frac{0}{i} + \cdots + - + \cdots + \frac{0}{j} + \cdots\rangle) \\
& (6 + 6 \cdot \frac{L-4}{2} + 6 \cdot \frac{L-6}{2}) \sum_{i \text{ even}} (|\cdots - \frac{0}{i} - 0 - \cdots\rangle + |\cdots + \frac{0}{i} + 0 + \cdots\rangle)] \tag{34}
\end{aligned}$$

we then find that $\delta_3^{II} = \|H_{II}^-|v_3\rangle - \beta_3|v_2\rangle\| = \frac{50(2L-9)}{(2L-5)(6L^2-45L+95)}$.

FSA for Model-III

In Model-III the $|00\rangle$ and $|++\rangle$ type of configurations are forbidden but $|+\rangle$ and $|0\rangle$ can sit next to each other. We start by

$$H_{III}^+|\mathbb{Z}_2\rangle = \frac{1}{\sqrt{2}} (\sum_{i \text{ even}} |\cdots - \frac{0}{i} - \cdots\rangle + \sum_{i \text{ odd}} |\cdots - + \frac{0}{i} + - \cdots\rangle) \tag{35}$$

So $\beta_1 = \sqrt{\|H_{III}^+|\mathbb{Z}_2\rangle\|} = \sqrt{L/2}$ and $|v_1\rangle = \frac{1}{\beta_1}H_{III}^+|\mathbb{Z}_2\rangle$. We checked that $H_{III}^-|v_1\rangle = \beta_1|\mathbb{Z}_2\rangle$ and hence $\delta_1^{III} = 0$.
Next

$$\begin{aligned}
H_{III}^+|v_1\rangle = & \frac{1}{\sqrt{2L}} (\sum_{i \text{ even}} |\cdots - \frac{-}{i} - \cdots\rangle + 2 \sum_{\substack{i,j \text{ even} \\ i \neq j}} |\cdots - \frac{0}{i} - \cdots - \frac{0}{j} - \cdots\rangle + 2 \sum_{\substack{i \text{ even} \\ j \text{ odd}}} |\cdots - \frac{0}{i} - \cdots + \frac{0}{j} + \cdots\rangle + \\
& 2 \sum_{\substack{i,j \text{ odd} \\ i \neq j}} |\cdots + \frac{0}{i} + \cdots + \frac{0}{j} + \cdots\rangle) \tag{36}
\end{aligned}$$

counting distinct number of 4 different type of states in Eq.(36), we get $\beta_2^2 = \frac{1}{2L}[\frac{L}{2} + 4 \cdot \frac{L}{4}(\frac{L}{2} - 1) + 4 \cdot \frac{L}{2}(\frac{L}{2} - 2) + 4 \cdot \frac{L}{4}(\frac{L}{2} - 1)] = L - \frac{11}{4}$. $|v_2\rangle = \frac{1}{\beta_2} H_{III}^+ |v_1\rangle$.

Next we find

$$H_{III}^- |v_2\rangle = \frac{1}{\sqrt{L(4L-11)}} [(2L-5) \sum_{i \text{ even}} |\dots - \underset{i}{0} - \dots\rangle + (2L-6) \sum_{i \text{ odd}} |\dots + \underset{i}{0} + \dots\rangle] \quad (37)$$

clearly $H_{III}^- |v_2\rangle$ is not equal to $|v_1\rangle$ multiplied by β_2 and this produces error in the 2nd FSA step. The norm of the difference is given by

$$\delta_2^{III} = \||H_{III}^- |v_2\rangle - \beta_2 |v_1\rangle\| = \frac{1}{4(4L-11)} \quad (38)$$
